Zhao, Wenli; Jama, Mohamed ; Buffo, Antonio; Alopaeus, Ville

Population balance model and experimental validation for reactive dissolution of particle agglomerates

Published in:
Computers and Chemical Engineering

DOI:
10.1016/j.compchemeng.2017.09.019

Published: 01/01/2018

Document Version
Peer-reviewed accepted author manuscript, also known as Final accepted manuscript or Post-print

Population balance model and experimental validation for reactive dissolution of particle agglomerates

Wenli Zhao[a, *], Mohamed Ali Jama[a], Antonio Buffo[b], Ville Alopaeus[a]

[a] *School of Chemical Technology, Aalto University, Kemistintie 1, 02150 Espoo, Finland*

[b]*Department of Applied Science and Technology, Politecnico di Torino, Corso Duca degli Abruzzi 24, 10129 Torino, Italy*

Abstract

We propose a population balance model coupled with a mass transfer model to simulate the simultaneous shrinkage and breakage of particles during the reactive dissolution of particle agglomerates in stirred tank. The high-order moment-conserving method of classes is adopted to solve the population balance model. In the mass transfer model, the driving force is estimated by considering the physical constraints including electroneutrality, water dissociation and dissolution equilibrium. The simulation results, including the concentration and the particle size distribution of the final products, were validated by experiments carried out in a laboratory scale stirred tank. The unknown physical parameters in the particle breakage model were fitted against the experimental data. The results underline the importance of particle breakage in the reactive dissolution modeling under the investigated operating conditions. Several daughter size distributions functions found in literature were tested. Among them, the beta distribution provides the most flexible way to describe breakage of the particle agglomerates.

Keywords: Reactive dissolution; Population balance; Electroneutrality; Particle breakage, High order moment conserving method of classes

* Corresponding author. Tel.: +358 45 1674316
E-mail address: zhao.wenli@hotmail.com (W. Zhao)

1. Introduction

Several efforts have been devoted to the experimental and numerical studies on solid-liquid reactive dissolution in various industrial applications such as reduction of metallic oxides, hydrometallurgy, kraft pulping, chemical leaching and aqueous mineral carbonation (Aydogan et al., 2005; Bandi, 1990; Grénman et al., 2010; Hövelmann et al., 2012; Kolodziej and Adamski, 1990). Three steps are involved in the reactive dissolution: the first step is mass transfer of the reactants from the bulk solution to the solid-liquid interface; the second step is surface reaction between the liquid reactant and solid reactant; the last step is mass transport of the product from the solid-liquid interface to the bulk solution. The slowest step exerts a dominating influence on the overall dissolution rate.

Shrinking particle model is usually employed to describe the solid-liquid mass transfer during the dissolution of non-porous powder particles. It is commonly based on the assumption that particles are monodispersed, i.e., all the particles have the same diameter(Levenspiel et al., 1999). Several analytical expressions of dissolution rates in the special cases where a single mechanism is rate limiting step, namely mass transfer control or surface reaction control, have been reported in the literature(Dickinson and Heal, 1999; Grénman et al., 2011). In reality, the polydispersity of the raw materials has a strong influence on the dissolution behavior: models formulated in terms of the average particle size can lead to large errors in the prediction of the realistic dissolution rate(LeBlanc and Fogler, 1987, 1989). Therefore, Leblanc and Fogler (1987) first developed the analytical expression for the dissolution rate of solids with polydispersity, which is limited by the assumption of constant liquid concentration and single rate limiting regime. Then a more general form of expression for the dissolution rate, which combined the models of mass transfer and surface reaction controlling regime, was proposed by Bhaskarwar (1989). On one hand, the actual particle size significantly affects the solid-liquid mass transfer coefficient. On the other hand, the particle size distribution (PSD) itself is essential to determine the interfacial area, especially in case of complex surface reactions. In the multiphase precipitation of $Mg(OH)_2$(s)-CO_2(g)-H_2O(l) system, for instance, the total solid surface area calculated from PSD of the dissolving particles could

provide the crystal growth area for the simultaneous crystallization process(Hövelmann et al., 2012; Zhao et al., 2016). Another example is the solid-liquid catalytic reaction, where the variation of the PSD of solid catalyst due to the chemical or mechanical process plays an important role in the mechanisms of catalyst deactivation(Bartholomew, 2001).

The solid-liquid mass transfer of uncharged molecules can be described by the typical Noyes-Whitney equation(Noyes and Whitney, 1897). For the reactive dissolution, the mass transfer rate is instead determined by the transport of charged ions. Therefore, the electroneutrality of the mass transfer fluxes must be satisfied during the dissolution of particles in electrolyte solutions. This aspect can be addressed by introducing the Nernst-Planck equation, which is capable of calculating the flux of ions under the influence of both ionic concentration gradient and electric field(Newman, 1991). Thus, the transports of cations and anions of all the components are taken into account in the mass transfer model. In addition, the solid-liquid interface concentrations are commonly calculated from the solubility of the component. However, Ji et al. proposed that the interface concentration could be lower than the saturated concentration, and this concentration difference could affect the prediction of dissolution rate(Ji et al., 2001). Therefore, it is interesting to see whether the interface concentration can be estimated by rigorous physical constraints rather than a simple saturated concentration.

Another important but often neglected phenomenon, is the breakage of the particles due to high shear rates occurring in the reactors (most commonly stirred tanks) where the dissolution process takes place. The raw materials are not always perfect spheres or cubes, but rather agglomerates with various morphology, and the breakage of such large agglomerates may alter the total solid-liquid contact area, influencing the dissolution rate in both mass transfer and surface reaction regimes. For this reason, a detailed population balance equation (PBE), accounting for both particle shrinking due to chemical dissolution and particle breakage due to intensive turbulence, is needed to properly describe the behavior of the dissolution process(Hänchen et al., 2007).

As the most important character of the dispersed phase in the multiphase processes, the variation of PSD caused by physical mechanisms including nucleation, growth, agglomeration and breakage can be described by solving population balance equation (PBE)(Randolph and Larson, 1988). However, for the reactive dissolution process under investigation, only the growth and breakage terms are relevant. Although the analytical solution of the PBE exists under limited and well defined simplified cases, for the realistic physical process, efficient numerical techniques are required to solve the PBM. Among many different approaches, the method of classes emerged as a valuable tool to predict the PSD in particle-based processes(Vanni, 2000). The most popular numerical scheme belonging to the method of classes family is the so-called fixed-pivot technique. It predicts the exact PSD of raw material by conserving two distribution moments (Kumar and Ramkrishna, 1996a, 1996b). The accurate solution of such low order approach, however, is only conserved by using a large number of classes, which may be unacceptable when PBM is coupled with Computational Fluid Dynamics (CFD) simulations or when the PBM is used to formulate and test new sub-models. Therefore, the low order fixed-pivot approach was extended by conserving defined number of moments of the distribution, leading to the high-order moment method of classes (HMMC)(Alopaeus et al., 2006, 2007). Comparing to the traditional numerical methods, HMMC offers accurate solution with considerably lower number of classes, as well as tracks the actual shape of PSD directly. Moreover this method is very flexible, since it allows to preserve an arbitrary set of moments, as well as a different number of internal variables of the population balance equation(Buffo and Alopaeus, 2016).

In this work, we propose a population balance model coupled with a mass transfer model to simulate the reactive dissolution of $Mg(OH)_2(s)$ in aqueous HCl solution. The surface reaction between H^+ and OH^- is a typical diffusion controlled reaction, in which the external mass transfer is the rate-controlling step(Tinoco et al., 1995). The growth term described by the mass transfer model is calculated by the Nernst-Planck equation. For the particle breakage term, a semi-theoretical power-law function is adopted to predict breakage rate while beta distribution is introduced as the daughter size distributions (DSD) function to describe particle size changes. In parallel with the modeling work, reactive dissolution experiments were carried out in a laboratory scale stirred tank reactor with different initial and operating conditions and the obtained experimental data were used to

verify and validate the model. Eventually, the empirical parameters including the breakage rate constant and the parameter of beta distribution were fitted against the experimental data.

2. Mathematical Modelling

The reactive dissolution of $Mg(OH)_2$ solids in aqueous HCl solution can be expressed as:

$$Mg(OH)_2(s) + 2HCl(aq) \rightarrow MgCl_2(aq) + 2H_2O \quad (1)$$

The shrinking particle model can be adopted to calculate the solid-liquid mass transfer during the reactive dissolution as shown in Figure. 1(a) (Levenspiel et al., 1999). Meanwhile, breakage of particle agglomerates will also affect the mass transfer area significantly in the stirred tank reactor as in Figure. 1(b). Consequently, the mass and population balance models, including the shrinkage and breakage of particles, are needed to describe the dissolution rate and the evolution of PSD based on the following assumptions:

1) The dissolving particles are spherical. The particle shrinks uniformly and maintains the same shape during the dissolution and breakage.
2) The liquid volume, V_L, is constant.
3) The agglomeration of the particles is neglected during the reactive dissolution.
4) Perfect mixing is assumed in the laboratory scale stirred tank reactor.

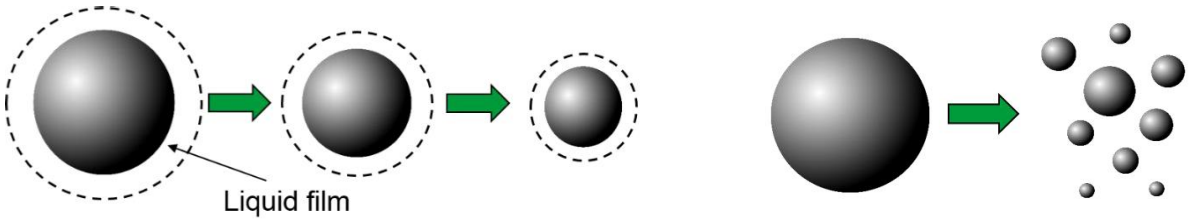

(a) Shrinkage of particle (b) Breakage of particle

Fig.1. Graphical representation of different phenomena occurring during the reactive dissolution.

It is important to mention that assumption of particle shape should be confirmed by experimental evidences, since the shape of raw materials could vary case by case. In this study, it is reasonable to assume agglomerates of

$Mg(OH)_2$ as spherical particles, according to the experimental observations performed through Scanning Electron Microscope (SEM).

2.1 Mass balance

As a rate-limiting step, the mass transfer rates of the components (Mg^{2+}, H^+, Cl^-, OH^-) between the solid-liquid interface and bulk solution determine the reactive dissolution rate. The liquid phase mass balance equation is:

$$\frac{dm_p}{dt} = N_p A_{tot} \tag{2}$$

where p is the index of chemical component; m_p is the amount of component dissolved in the liquid phase, mol; N_p is the mass transfer flux, mol/(m^2s); A_{tot} is the total solid-liquid mass transfer area, m^2.

The solid-liquid mass transfer flux can be calculated as (Zhao et al., 2016):

$$N_p = k_{s,p}\Delta c_p - k_{s,p} z_p \overline{c_p}\left[\frac{\sum_p (z_p k_{s,p}\Delta c_p)}{\sum_p (z_p{}^2 k_{s,p}\overline{c_p})}\right] \tag{3}$$

where $k_{s,p}$ is the size dependent solid-liquid mass transfer coefficient, m/s; z are the charges of the cationic and anionic species; Δc_p and $\overline{c_p}$ are the concentration difference and average concentration between the solid-liquid interface and the bulk solution respectively, mol/m^3. The first term on the RHS of the Eq. (3) is the typical mass transfer flux, while the second term on the RHS is derived from the Nernst-Planck equation to preserve the electroneutrality of mass transfer flux during the dissolution of particles in the electrolyte solution**.**

To calculate the concentration difference between the solid-liquid interface and the bulk solution, the interface concentrations are needed. As previously mentioned, the solid-liquid interface concentration is usually assumed constant determined by solubility product. Then, the interface concentration of components, including Mg^{2+}, Cl^-, H^+ and OH^-, are 54.89, 107.15, 5.46×10^{-7} and 0.018 mol/m^3 respectively. In this study, alternatively, we estimate

the solid-liquid interface by simultaneously considering the physical constraints including electroneutrality (Eq. (4)), water dissociation (Eq. (5)) and dissolution equilibrium (Eq. (6)):

$$c_{H,interface} + 2c_{Mg,interface} = c_{OH,interface} + c_{Cl,interface} \quad (4)$$

$$c_{H,interface} c_{OH,interface} = K_w \quad (5)$$

$$c_{Mg,interface} c_{OH,interface}^2 = K_{sp} \quad (6)$$

where K_w and K_{sp} are the water auto-ionization constant and the solubility product of $Mg(OH)_2$ at 25ºC. The bulk concentration of chloride remains constant during the dissolution as it is not added to the system. Therefore, the mass transfer flux of chloride (N_{Cl}) can be assumed to be zero, which is an additional fourth constraint to Eqs. (4)-(6). The interface concentrations of components are not assumed constant, but calculated numerically according to the physical constraints (from Eq. (3) to Eq. (6)) at every time step.

The solid-liquid mass transfer coefficient, $k_{s,p}$, is influenced by the mixing condition, geometry and position of the impeller and the particle diameter. For particles with a wide size range in stirred tank reactor, $k_{s,p}$ can be calculated by the following correlation (Asai et al., 1989):

$$Sh_p = \left[2^{5.8} + \left(0.61 Re_\varepsilon^{\,0.58} Sc_p^{\,1/3} \right)^{5.8} \right]^{1/5.8} \quad (7)$$

where Sh_p is the Sherwood number; Re_ε is the particle Reynolds number; Sc_p is the Schmidt number. There are many ways to define the particle Reynolds number: in this case the inertial contribution is mainly caused by the movement of the impeller in a stirred tank reactor. Therefore, the Re_ε is calculated based on the energy dissipation rate and particle size (Levins and Glastonbury, 1972):

$$Re_\varepsilon = \left(\varepsilon_T L^4 \right)^{1/3} / \nu_L \quad (8)$$

where ε_T is the overall energy dissipation rate, m^2/s^3; L is the particle size, m; ν_L is the kinematic viscosity of liquid, m^2/s. The Sh_p and Sc_p are component-dependent dimensionless numbers which can be estimated as:

$$Sh_p = k_{s,p} L / D_p \tag{9}$$

$$Sc_p = \mu_L / \left(\rho_L D_p\right) \tag{10}$$

where D_p is the diffusion coefficient of component p, m^2/s; μ_L is the dynamic viscosity of the liquid, $P_a s$; ρ_L is the density of the liquid, kg/m^3. PSD needed for estimation of the dimensionless numbers and total mass transfer area can be obtained by solving the population balance model.

2.2 Population balance

As previously mentioned, the only particle size related physical phenomena considered here are the particle shrinkage and the particle breakage. The population balance equation (PBE) can be written for particle diameter (L) as the internal coordinate as:

$$\frac{\partial\left(n\left(L,t\right)\right)}{\partial t} = \int_L^\infty \beta\left(L,\lambda\right) g\left(\lambda,t\right) n\left(\lambda,t\right) d\lambda - g\left(L,t\right) n\left(L,t\right) + \frac{\partial\left(G\left(L,t\right) n\left(L,t\right)\right)}{\partial L} \tag{11}$$

where $n(L, t)$ is the number density, $\#/m^4$; $\beta(L, \lambda)$ is the daughter size distribution (DSD); $g(L, \lambda)$ is the breakage frequency, 1/s; $G(L, t)$ is the growth rate, m/s. The LHS of the Eq. (11) represents the time rate of change of the number density function (NDF). The first and second RHS terms describe the birth and death of the particles due to breakage, respectively. The last term represents the growth rate of particles which is negative due to the particle shrinkage.

The PBE can be solved with the method of classes (MC), where the internal coordinate space is discretized into a finite number of size classes (NC) and the number density of particle (Y_i) belonging to each class is counted. By transforming the integral term (e.g., breakage) and hyperbolic partial differential term (e.g., growth) into their discrete counterparts, Eq. (11) becomes the following (coupled) set of ordinary differential equations:

$$\frac{dY_i}{dt} = \sum_{j=1}^{NC} B\left(L_i, L_j\right) g\left(L_j\right) Y_j - g\left(L_i\right) Y_i + \sum_{j=1}^{NC} \xi\left(L_i, L_j\right) G\left(L_j\right) Y_j \tag{12}$$

where i and j are the indices of particle size class; Y_i is the particle number density of each class, #/m^3; $B(L_i, L_j)$ is the breakage table; $\xi(L_i, L_j)$ is the growth table. The breakage and growth tables are built to calculate the contribution of new formed particles to the whole discretized distribution. For the original method to describe the contribution, the reader may refer to the specialize literatures(Kumar and Ramkrishna, 1996a, 1996b). Note that the tables usually depend only on the discretization of the internal coordinate and remain the same during the time integration. Therefore, the tables can be calculated in advance, significantly reducing the computational load, especially when PBE is coupled with CFD calculations. In this respect, the High-order Moment Method of Classes (HMMC) offers an efficient way of constructing the tables of $B(L_i, L_j)$ and $\xi(L_i, L_j)$ (Alopaeus et al., 2007, 2006). In order to solve the population balance model with HMMC for the system under investigation, several sub-models including growth rate, breakage frequency and daughter size distribution are needed.

2.2.1 The Growth term

The growth term (third RHS term of Eq. (12)) is constituted of two parts: the growth rate that depends on the physical properties during the time integration ($G(L_i)$) and the growth table that depends only on the discretization of the internal coordinate ($\xi(L_i, L_j)$). For a particle with size L_i, the growth rate is function of the mass transfer flux and the particle size. It can be derived from Eq. (2):

$$G(L_i) = \frac{N_p(L_i) A(L_i) v_m}{3 k_v L_i^2} \tag{13}$$

where $N_p(L_i)$ is mass transfer flux for particle with size L_i, mol/(m^{2}s); $A(L_i)$ is the particle surface area, m^2; k_v is the volume shape factor (equal to $\pi/6$ for spheres); v_m is the molar volume of solid, m^3/mol. The growth table is built to distribute the growth of particle with particular size class into a number of neighboring classes. Then the contribution of growth is summed to cover the whole discretized distribution. The construction of the growth table can be done before the time integration of Eq. (12). In this study, the growth of the smallest particles are not distributed to other classes since they disappear completely upon further dissolution. Instead, the dissolution

appears as a sink term of PBE just like negative nucleation. Therefore, the growth term for the particles in the first class should be redefined to describe the disappearance of the particles:

$$\xi(L_1, L_1) G(L_1) Y_1 = \frac{N_p(L_1) A_{tot}(L_1)}{n(L_1) V_{disp}} \tag{14}$$

where $A_{tot}(L_1)$ is the total area of the particles in the first class, m^2; $n(L_1)$ is the mass of the single particle in the first class, mol; V_{disp} is the volume of dispersion, m^3. Then the first element in the breakage table becomes:

$$\xi(L_1, L_1) = \frac{3}{L_1} \tag{15}$$

2.2.2 The Breakage term

The birth term by particle breakage can also be factored into two part: $g(L_j)$ is the breakage frequency for the particle of size L_j, while $B(L_i, L_j)$ describes the probability that a fragment of size L_i formed due to the breakage of particle with size L_j. The breakage frequency is a function which relies on different physical parameters of the investigated system, e.g., turbulent dissipation rate, liquid viscosity and size of the breaking particle. The breakage of particle agglomerates was reported to strongly depend on the ratio between the particle size and the smallest turbulent eddy(Marchisio and Fox, 2013). Therefore, the breakage law can be presented in terms of well-known quantities, namely diameter of the particle agglomerate (L_i), the Kolmogorov length scale (η), and Kolmogorov time scale (η_T) (Zhao et al., 2017):

$$g(L_i) = \psi_{br} \left(\frac{L_i}{\eta} \right)^{\gamma} \eta_T^{-1} \tag{16}$$

where ψ_{br} and γ are dimensionless empirical constants. Peng and Williams found that γ can be assumed to be between 1 and 3(Peng and Williams, 1994). In this work, γ is assumed to be 1 and ψ_{br} is obtained by parameter fitting against experimental data. In addition, the particle-particle and particle-wall collision determined by the flow field was reported to have strong effect on the particle behavior in a stirred tank with volume of 10L and

solid volume fraction of 10%(Hartmann et al., 2006). In this study, however, the volume of liquid and volume fraction of solids are 2.5L and 0.17% respectively. Therefore, the particle-particle and particle-wall collision were ignored and perfect mixing was assumed.

Together with the breakage frequency, also the daughter size distribution (DSD) function is needed to model the outcome of a breakage event. A variety of functional forms for the DSD functions has been proposed and validated through comparison with the experimental data. Most of the DSD functions are proposed based on the breakage of single particle, droplet and bubbles(Luo and Svendsen, 1996; Zaccone et al., 2007). Kramer and Clark summarized the breakage mechanisms of particle agglomerates and proposed the model of breakage frequency ($g(L_i)$)(Kramer and Clark, 1999). For the particle agglomerate, however, many factors such as the structure of the particle agglomerates, the strength of particle-particle bridges and the breakage pattern should be considered in the formulation of the DSD. Unfortunately, a comprehensive study on DSD functions for the breakage of particle agglomerates is not available in the literature. An empirical way adopted in this work to overcome this issue is to introduce a well-defined probability density function form with a limited number of parameters controlling the shape of the distribution and the number of the fragments generated by the breakage event, which can be fitted through comparison with the experiments. For this purpose, beta distribution is a suitable continuous probability distributions function which has been used to empirically describe the breakage of bubbles in the literature (Laakkonen et al., 2007):

$$\beta\left(L_i, L_j\right) = \frac{1}{2}(1+a)(2+a)(3+a)(4+a)\left(\frac{L_i^2}{L_j^3}\right)\left(\frac{L_i^3}{L_j^3}\right)^2\left(1-\frac{L_i^3}{L_j^3}\right)^a \tag{17}$$

where a is the adjustable parameter of beta distribution. It is desirable to integrate the DSD function analytically in order to avoid numerical errors and reduce the computational cost in the construction of breakage table. For the beta distribution, however, the numerical integration is the only option due to the complex formation. Because it is sufficient to build the breakage table only once before the time integration, workload is not an issue

and tight integration tolerances can be adopted. It should be noticed that the total volume of the daughter particles is equal to the mother particle. In another word, the volume of mother particle is conserved during the numerical integration of beta distribution (Eq. (17)).

Note that the breakage rate constant and the parameter of beta distribution are tank average values which are obtained by parameter fitting based on the assumption of spatial homogeneity of the laboratory scale reactor. In the stirred tank reactor, the breakage rate of particle agglomerates near the impeller could be larger than the tank average value due to the non-uniform distribution of the turbulent intensity, as well as the PSD can be different from point to point in the domain. Indeed, a fitting process that involves the influence of hydrodynamics, mainly taking the local energy dissipation rate into account, could result in a more applicable and realistic set of physical parameters (ψ_{br} and a) . However, the aim of this work is to formulate a simple model that helps us in the understanding of the investigated process; a detailed CFD model of the reactive dissolution is outside the scope of the present work and left for the future.

2.3 Numerical details

The mathematical model consisting mass balance equations and population balance equations was implemented in Matlab R2016b. For the mass transfer model, the solid-liquid interface concentration is calculated numerically with the Levenberg-Marquardt algorithm at every time step (Marquardt, 1963). For the population balance model, 60 classes were applied to the internal-coordinate space (particle size) with a discretization based on a geometric series. Six moments were chosen to be conserved during the construction of breakage table and growth table. The ordinary differential equations coupling the mass balance and population balance models were integrated by using the variable-step and variable-order Backward Differencing Formula (BDF) algorithm, namely ode15s. To reduce the influence of the numerical errors associated with the time integration, a tight tolerances (RTOL=1E-10, ATOL=1E-12) were adopted.

3. Experimental apparatus and operating conditions

The experimental system consisted of a 3L jacketed glass stirred tank equipped with a Rushton turbine impeller, a thermostat (Lauda T2200) and an on-line pH meter (Metrohm 744). In order to improve mixing and prevent vortex formation, four baffles were located symmetrically at the inner wall of the reactor. In each batch operation, 2.5L HCl solution (pH ≈ 1) was first mixed in the reactor at 25°C. When the temperature and pH achieved stable values, Mg(OH) solids were rapidly added into the solution. The dissolution rate can be obtained by tracking the concentration of magnesium ion with ion chromatography (ICS-1100) at different times, or by monitoring the pH. Unfortunately, based on the separate tests, the response time of pH meter was around 15s which is too slow to follow the reactive dissolution. The PSD of the final products were analyzed by a Mastersizer 3000 laser diffraction analyzer.

Table 1. Initial and operating conditions

No.	Sample	Impeller speed, rpm	Initial pH	Initial mass of solids, g
Case 1	1	560	1.01	10.04
Case 2	2	560	0.97	10.09
Case 3	2	360	0.98	10.01

In order to validate the proposed model, different initial conditions (particle sizes) and operation conditions (impeller speeds) applied for the experiments were listed in Table 1. For the raw material, it is difficult to validate the dissolution rate due to the present of a mass of fine particles that dissolves extremely rapidly. Therefore, the two larger samples were obtained by mechanical sieving. The influence of initial conditions on the reactive dissolution can be found by carrying out the tests with different sieved samples and identical impeller speed (Case 1 vs Case 2) while the effect of operating conditions on the reactive dissolution can be revealed by performing the tests with the same sample but different impeller speeds (Case 2 vs Case 3). In addition, the fully suspended stirring speed, N_{mix}, is an empirical and highly case dependent variable determined by the geometry of tank and impeller, the position of the impeller, particle diameter and particle mass fraction(Paul et al., 2004). In this work, N_{mix} was measured experimentally in the $Mg(OH)_2$(s)-H_2O system with

the present sample: the classification of particles disappears when the impeller speed was above 350rpm. Consequently, the impeller speeds were 360 rpm and 560 rpm in the experiment.

4. Results and discussion

4.1 Discretization of the initial PSD

As the proper description of the initial condition is essential in the solution of the ODEs constituting the PBM, the accurate discretization of the initial PSD is crucial to model the reactive dissolution. The SEM pictures of the raw materials of $Mg(OH)_2$ particles are reported in Figure 2. Fig.2 (a) shows that the raw materials are polydispersed particle mixture with roughly spherical shape, providing the feasibility of the assumption on the agglomerate shape. The enlargement of the same sample (Fig.2 (b)) shows the morphology of the particles. A high degree of the agglomeration in the raw material can be observed on a smaller spatial scale, demonstrating the fact that the breakage event can produce particles with a wide size range.

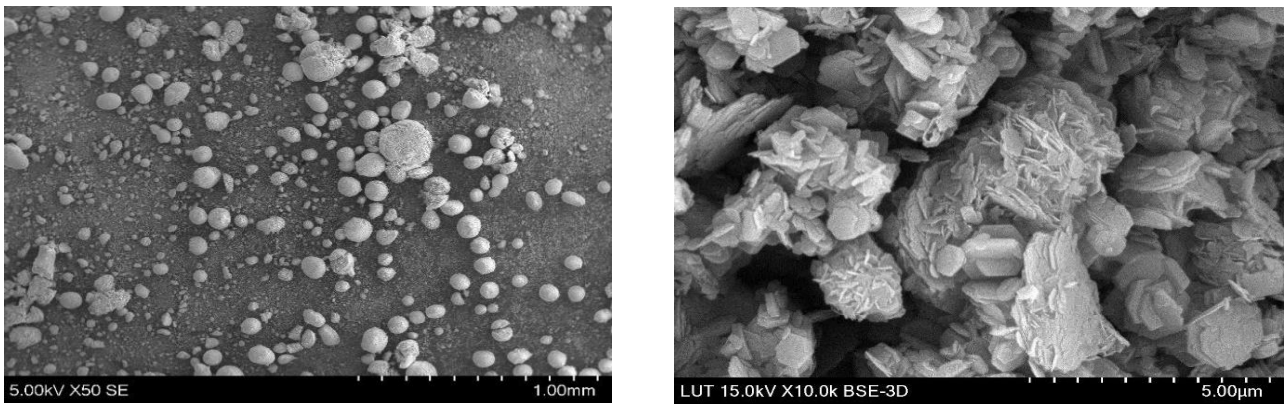

(a) $Mg(OH)_2$ (scale bar 1mm) (b) $Mg(OH)_2$ (scale bar 5µm)

Fig.2. Characteristic SEM images of raw particle material

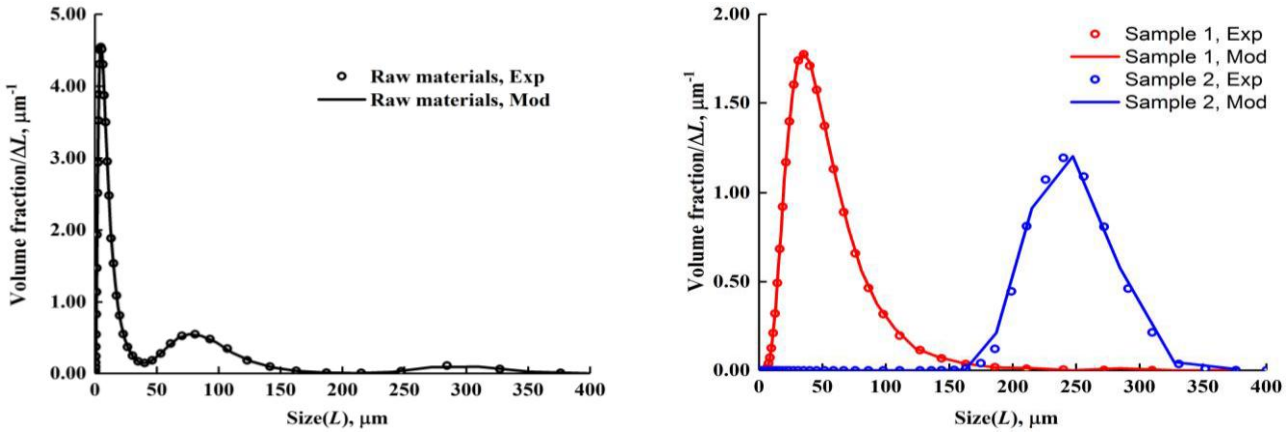

(a) Raw materials (b) Sieved materials

Fig.3. Initial PSD of the $Mg(OH)_2$ particles

The initial PSD of particles is usually obtained by using a predetermined probability density function (PDF) such as lognormal or Weibull distribution in which parameters are fitted against measured PSD (Leblanc and Fogler, 1987). The high degree of polydispersity of the raw materials in Fig. 3 (a), however, may lead to deviations between the fitted and measured initial PSD, which introduces further modelling errors. Therefore, the moment-conserving discretization of the initial PSD is performed(Ahmad et al., 2015). The main idea of discretization is to distribute the measured PSD into the predefined size classes, which can give excellent prediction of not only the shape, but also of the moments of the initial PSD in Fig. 3.

4.2 The influence of operating conditions on the reactive dissolution

The concentration of magnesium ion and the PSD of the final products were calculated and compared with the experimental results under different initial and operating conditions. The only unknown physical parameters including the particle breakage constant (ψ_{br}) and the parameter of the DSD function were fitted against the experimental data, and the results of this procedure are reported in Table 2.

Table 2 Breakage rate constant and parameter of beta distribution

Parameter	Value (95% confidence interval)
ψ_{br}	$1.12\times10^{-5} \pm 9.82\times10^{-7}$
a	$1.35\times10^{2} \pm 7.42$

The dissolution rate can be calculated from the time evolution of the magnesium ion concentration in Fig.4 (a). It shows that the dissolution rate increases when the impeller speed increases or the initial particle size decreases: such rate is in fact governed by the solid-liquid mass transfer rate, which consists of three different terms, namely the mass transfer coefficient, the mass transfer area and the dissolution driving force. Compared with the typical non-reactive dissolution process, this case still presents relatively high dissolution rates in spite of the reducing driving force. The effect of PSD and turbulent energy dissipation on the solid-liquid mass transfer coefficient and, therefore, on the total mass transfer area is clear in Fig.4 (b) and Fig.4 (c): the total mass transfer area is the highest in Case 1, where the initial PSD is shifted towards smaller particle diameters and where the impeller speed are constant. By observing Case 2 and Case 3, it is possible to note that a stronger turbulent intensity caused by the faster impeller speed results in a higher mass transfer rate, with a combined effect provided by an enhanced mass transfer and a higher particle breakage rate. In fact, in Case 2 a large amount of fine particles generated by the agglomerate breakage can speed up the dissolution as compared with Case 3, by providing a larger interfacial area for mass transfer.

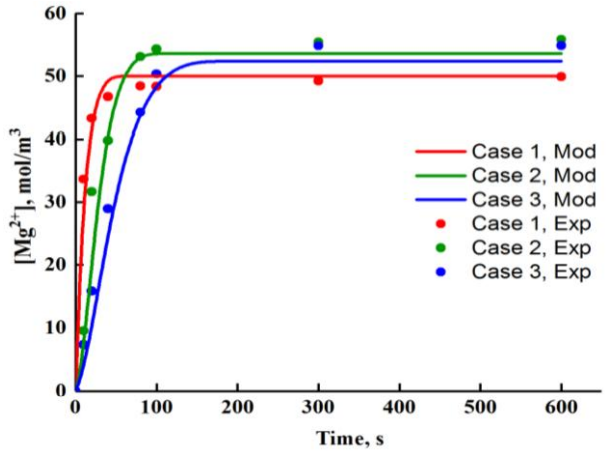

(a) Concentration of Mg^{2+}

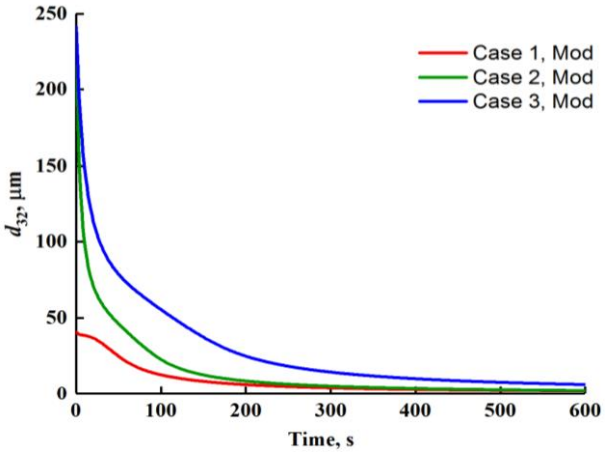

(b) Mean Sauter diameter

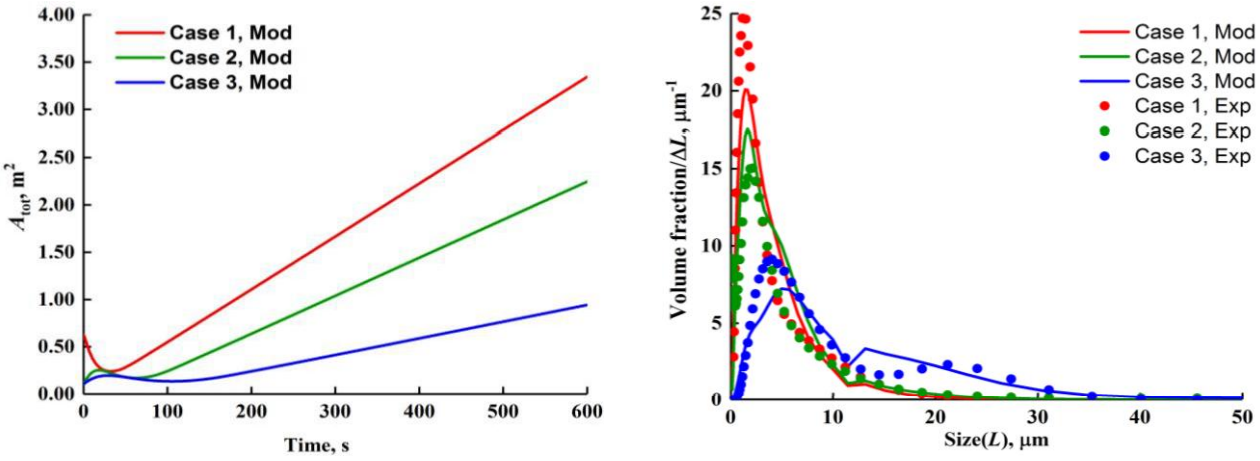

(c) Total solid-liquid mass transfer area (d) PSD of the final products after 600s

Fig.4. Modelling vs Experimental results

In addition, the present model can give a better understanding of reactive dissolution by analyzing the influence of operating conditions on both particle diameter and mass transfer area. The Sauter Mean Diameter (d_{32}) of the particles and the solid-liquid mass transfer area (A) are shown in Fig.4(b) and Fig.4(c). Case 1 produces the particles with smallest d_{32} and largest A, which results in a highest mass transfer rate, while Case 3 produces the particles with the largest d_{32} and smallest A, which results in a lowest mass transfer rate. These results agree with the experimental data in Fig. 4(a). Compared with Case 2 and Case 3, it is worth noting that the mass transfer area decreases in Case 1 in the first 40 s and then increase as depicted in Fig. 4(c). In theory, the mass transfer process reduces the mass transfer area according to the shrinking particle model while the particle breakage increases mass transfer area by generating fine particles. Therefore, it is can be deduced that the particle dissolution has a major influence on the solid-liquid mass transfer area of the smaller particles (Sample 1) while particle breakage dominates the evolution of mass transfer area of the large particles(Sample 2). The different tendency between d_{32} and A proves that the mass transfer rate cannot be predicted accurately by only tracking two moments of the distribution, which usually are the total number of particles and the total volume of the system. A proper prediction in fact requires also the inclusion of an additional moment accounting for the total interfacial area, and therefore the use of the HMMC for the solution of the PBE for mass transfer problems is favorable.

Table 3 The influence of initial particle size and impeller speed on d_{32} of the final products

No.	Impeller speed, rpm	Initial d_{32}, μm	Final d_{32}, μm (Experiment)	Final d_{32}, μm (Modelling)
Case 1	560	40.98	2.04	2.10
Case 2	560	241.75	2.52	2.47
Case 3	360	241.75	6.13	6.38

The experimental and modelling results of d_{32} of the sample taken at 600s are compared in Table 3. By looking at the values reported, it is possible to notice that the final particle size at the steady state is mainly determined by the impeller speed, with a negligible effect of the initial PSD. Furthermore, the present model can give a reasonable prediction of the PSD with the fitted physical parameters in Fig. 4(d).

4.3 The influence of breakage frequency and DSD function on the reactive dissolution

The influence of the impeller speeds on particle diameter and mass transfer area shows that particle breakage could play an important role in the reactive dissolution of particle agglomerate. The evolution of PSD simulated by the reactive dissolution model (Case 2) with and without breakage were compared in Fig. 5. The PSD calculated by the model without breakage is only controlled by the solid-liquid mass transfer. Since the mass transfer rate of the smaller particles is higher than the larger ones, the PSD slowly becomes wider in Fig. 5(a). This behavior is not consistent with the experimental data reported in Fig.4 (d). The results calculated by the model including breakage shows instead that such phenomenon rapidly shifts the PSD towards smaller particle diameters, as depicted in Fig. 5(b). Therefore, it is crucial to correctly describe the breakage of the agglomerations for the modeling of the present reactive dissolution. It should be noticed that the particle volume fraction in Fig.4 (d) is calculated based on the remaining solid volume at corresponding time step, for the purpose of comparison with the experimental data. In order to monitor the evolution total solid volume and PSD, the particle volume fraction is calculated based on the initial solid volume in Fig.5.

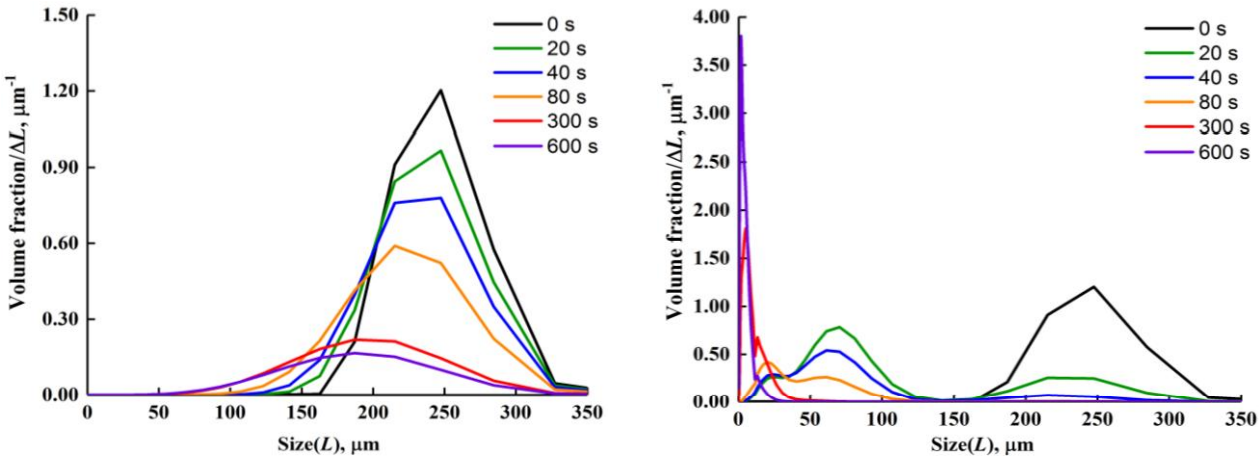

(a) Model without breakage (b) Model with breakage

Fig.5 Modelling results of PSD evolution (based on the initial solid volume)

Table 4 Breakage rate constants corresponding to the tested DSD functions

DSD functions	Value of ψ_{br} (95% confidence interval)
Beta (This study)	$1.12\times10^{-5} \pm 9.82\times10^{-7}$
Uniform	$9.83\times10^{-5} \pm 5.60\times10^{-6}$
Binary	$9.04\times10^{-5} \pm 1.33\times10^{-5}$
Symmetry	$5.47\times10^{-5} \pm 8.23\times10^{-6}$
Mass ratio 1:4	$1.02\times10^{-4} \pm 5.83\times10^{-6}$

As it is possible to see from Fig. 6(a), the model without breakage results in a large deviation from the experimental data, which again stresses the importance of the particle breakage in the modeling of reactive dissolution. Meanwhile, the DSD functions accounting for the number of fragments (and their sizes) generated after the breakage event must be properly selected in order to predict the PSD accurately. Several DSD functions summarized in the literature (Marchisio et al., 2003) were implemented into the population balance model. In order to investigate the influence of DSD functions, breakage rate constants (ψ_{br}) corresponding to the tested DSD functions were separately fitted against experimental data (in Table 4) to ensure the same dissolution rate. It is apparent that the breakage rate constant is related to the choice of the DSD function. The different DSD functions result in different PSDs of the final product in Fig. 6(b). It is worth remarking that the DSD highly depends on the investigated system, and in particular on the agglomerates internal stress and the interaction with

the hydrodynamics. Therefore the formulation of a phenomenological model can be very tricky, since the available experimental data are not sufficient for a more detailed validation. The prescribed beta distribution, instead, due to its flexibility compared with other imposed DSD, is able to provide a good agreement compared with the experimental data at different operating conditions (Fig. 4 (d)) by using a unique set of parameters. Nevertheless, since the structure and the strength of the particle agglomerates are case dependent, the breakage rate constant could be varying in different systems, although these results are promising from a modeling point of view.

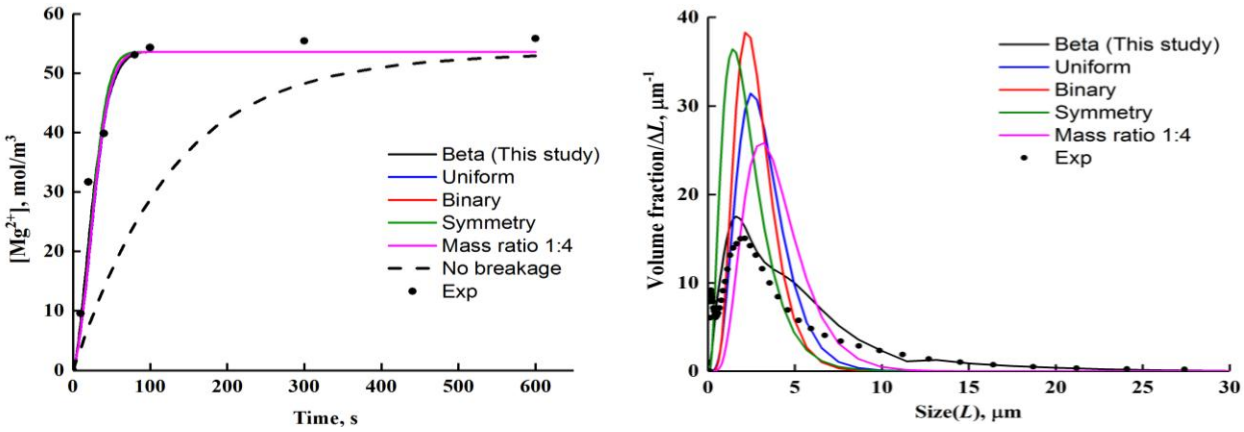

(a) Mg^{2+} concentration (b) PSD after 600s (based on remaining solid volume)

Fig.6. The influence of different DSDs on the PSD

4.4 The solid-liquid interface concentration

The interface concentration and mass transfer rate of components in Case 2 are presented in Fig.7 and Fig. 8. The interface concentration of OH^- and H^+ are supposed to be very low due to the instantaneous neutralization. Then the interface concentration of Cl^- is strongly influenced by Mg^{2+}, as the electroneutrality of interface concentration, Eq. (4), should be always satisfied. It is can be seen from Fig.7 that the interface concentration of Mg^{2+} and Cl^- are larger than the saturated concentration while the concentration of OH- is smaller than the saturated concentration. In addition, the concentration gradient of Cl^- between the bulk solution and solid-liquid interface exists during the reactive dissolution even though the mass transfer flux of Cl^- is zero. By introducing the Nernst-Planck equation, moreover, the conservation for the electroneutrality of the mass transfer flux is also

guaranteed in Fig.8. The mass transfer rate of Mg^{2+} increases at first 10s and then decreases. This is mainly caused by the small variation of mass transfer area in Fig. 4(c). It can be deduced that the accurate prediction of the mass transfer area, which is determined by the particle size distribution, is critical to the modelling of reactive dissolution. The time-dependent interface concentrations represent the major difference between the reactive dissolution and non-reactive dissolution. By considering the physical constraints (electroneutrality, water dissociation and dissolution equilibrium) and the transport of all the components, the model can provide a more feasible and accuate prediction of the mass transfer rate than the constant value samply calculated from the solubility equilibrium.

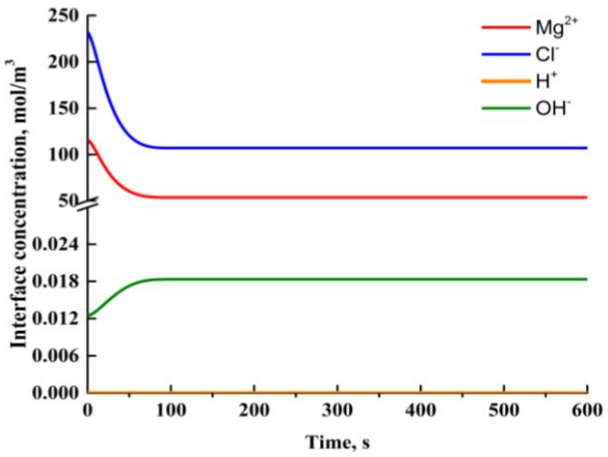

Fig.7. Interface concentration of components

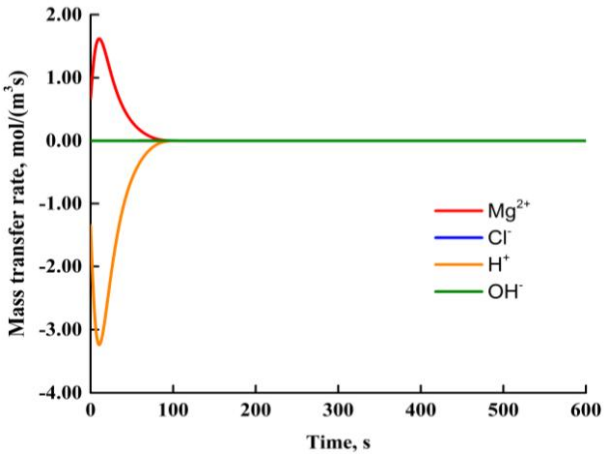

Fig.8. Mass transfer rate of components

5 Conclusions

This work proposed a mathematical model for reactive dissolution of solid agglomerates under ideal mixing assumption. The simultaneous particle shrinkage and breakage were described by using the population balance model coupled with a mass transfer model. In the mass transfer model, the Nernst-Planck equation is adopted to guarantee the electroneutrality of the mass transfer fluxes and the interface concentrations. To describe the breakage of agglomerates, beta distribution is adopted as a daughter size distribution function, while the breakage frequency is modeled with an empirical correlation that accounts for the interaction between particle

and turbulent eddy. The resulting population balance model is eventually solved by means of the high-order moment-conserving method of classes.

The comparison between the modeling results and the data measured during reactive dissolution experimental campaign carried out in a laboratory scale stirred tank reactor pointed out several interesting aspects. Firstly, the model is capable of predicting the influence of different initial particle size and impeller speed on the reactive dissolution rate. Then, the influence of particle breakage on the Sauter Mean Diameter and the mass transfer area were identified: the inclusion of the particle breakage in the model is crucial to the accurate simulation of the dissolution rate and the evolution of particle size distribution. Compared to several daughter size distributions in the literature, the beta distribution provided the most flexible way to predict the breakage of solid agglomerates with complex internal structures. Finally, the interface concentration estimated by considering the physical constraints including electroneutrality, water dissociation and dissolution equilibrium, was found to be different from the values calculated by the solubility equilibrium during the reactive dissolution.

Nomenclature

a	dimensionless shape factor of Beta distribution, [-]
A_{tot}	total mass transfer area, m^2
B	breakage table
c	concentration of component, mol/m^3
D	diffusion coefficient of component p, m^2/s
g	breakage frequency, 1/s
G	growth rate, m/s
k	mass transfer coefficient, m/s
K_{sp}	solubility product, mol^3/m^9
k_v	volume shape factor, [-]
K_w	water auto-ionization constant, mol^2/m^6
L	particle size, m
m	amount of component, mol
n	number density, $\#/m^4$
N	mass transfer flux, $mol/(m^2s)$
Re_ε	Reynolds number, [-]
Sc	Schmidt number, [-]
Sh	Sherwood number, [-]
V	volume, m^3

	v_m	molar volume, m^3/mol
	Y	paricle number density, #/m^3
	z	charge of the cationic and anionic, [-]
1	Greek letters	
	β	daughter size distribution function, [-]
	γ	exponent of the particle size in power-law breakage kernel, [-]
	ρ	density, kg/m^3
	η	Kolmogorov length scale, m
	η_T	Kolmogorov time scale, s
	ξ	*g*rowth table, m^{-1}
	μ	dynamic viscosity of the liquid, P_as
	ψ	breakage rate constant, [-]
	ε_T	overall energy dissipation , m^2/s^3
	ν	kinematic viscosity of liquid, m^2/s
2	Subscripts	
	br	breakage
	disp	dispersion
	i, j	index of the particle size classes
	L	Liquid phase
	p	index of the components
	s	solid phase
3		

4

5 **Acknowledgments**

6 Financial support from the Finnish Academy, project FLUKI (no. 13259597, no. 260141) is gratefully
7 acknowledged. The authors would like to sincerely thank Prof. Marjatta Louhi-Kultanen, Dr. Bing Han for the
8 help during the experimental validation and Mr. Toni Väkiparta for the SEM imaging.

9

10 **References**

11 Ahmad, W., Kuitunen, S., Sixta, H., Alopaeus, V., 2015. Population balance based modeling of changes in
12 cellulose molecular weight distribution during ageing. Cellulose. 22, 151–163.
13 Alopaeus, V., Laakkonen, M., Aittamaa, J., 2007. Solution of population balances with growth and nucleation by
14 high order moment-conserving method of classes. Chem. Eng. Sci. 62, 2277–2289.
15 Alopaeus, V., Laakkonen, M., Aittamaa, J., 2006. Solution of population balances with breakage and
16 agglomeration by high-order moment-conserving method of classes. Chem. Eng. Sci. 61, 6732–6752.
17 Asai, S., Konishi, Y., Kajiwara, T., 1989. Effect of sparged gas on mass transfer between fine particles and
18 liquids in an agitated vessel. J. Chem. Eng. Japan. 22, 96-98.
19 Aydogan, S., Aras, A., Canbazoglu, M., 2005. Dissolution kinetics of sphalerite in acidic ferric chloride leaching.
20 Chem. Eng. J. 114, 67–72.
21 Bandi, A., 1990. Electrochemical Reduction of Carbon Dioxide on Conductive Metallic Oxides. J. Electrochem.
22 Soc. 137, 2157–2160.

Bartholomew, C.H., 2001. Mechanisms of catalyst deactivation. Appl. Catal. A Gen. 212, 17–60.
Bhaskarwar, A.N., 1989. General population balance model of dissolution of polydisperse particles. AIChE J. 35, 658–661.
Buffo, A., Alopaeus, V., 2016. Solution of bivariate population balance equations with high-order moment-conserving method of classes. Comput. Chem. Eng. 87, 111–124.
Dickinson, C.F., Heal, G.R., 1999. Solid–liquid diffusion controlled rate equations. Thermochim. Acta 340–341, 89–103.
Grénman, H., Salmi, T., Murzin, D.Y., 2011. Solid-liquid reaction kinetics - Experimental aspects and model development. Rev. Chem. Eng. 27, 53–77.
Grénman, H., Wärnå, J., Mikkola, J.P., Sifontes, V., Fardim, P., Murzin, D.Y., Salmi, T., 2010. Modeling the influence of wood anisotropy and internal diffusion on delignification kinetics. Ind. Eng. Chem. Res. 49, 9703–9711.
Hartmann, H., Derksen, J.J., Van Den Akker, H.E.A., 2006. Numerical simulation of a dissolution process in a stirred tank reactor. Chem. Eng. Sci. 61, 3025–3032.
Hänchen, M., Krevor, S., Mazzotti, M., Lackner, K.S., 2007. Validation of a population balance model for olivine dissolution. Chem. Eng. Sci. 62, 6412–6422.
Hövelmann, J., Putnis, C. V., Ruiz-Agudo, E., Austrheim, H., 2012. Direct nanoscale observations of CO2 sequestration during brucite [Mg(OH)2] dissolution. Environ. Sci. Technol. 46, 5253–5260.
Ji, X., Chen, D., Wei, T., Lu, X., Wang, Y., Shi, J., 2001. Determination of dissolution kinetics of K2SO4 crystal with ion selective electrode. Chem. Eng. Sci. 56, 7017–7024.
Kolodziej, B., Adamski, Z., 1990. Dissolution of sphalerite in aqueous hydrochloric acid solutions under reduction conditions. Hydrometallurgy 24, 393–406.
Kramer, T.A., Clark, M.M., 1999. Incorporation of Aggregate Breakup in the Simulation of Orthokinetic Coagulation. J. Colloid Interface Sci. 216, 116–126.
Kumar, S., Ramkrishna, D., 1996a. On the solution of population balance equations by discretization—I. A fixed pivot technique. Chem. Eng. Sci. 51, 1311–1332.
Kumar, S., Ramkrishna, D., 1996b. On the solution of population balance equations by discretization—II. A moving pivot technique. Chem. Eng. Sci. 51, 1333–1342.
Laakkonen, M., Moilanen, P., Alopaeus, V., Aittamaa, J., 2007. Modelling local bubble size distributions in agitated vessels. Chem. Eng. Sci. 62, 721–740.
Leblanc, S.E., Fogler, H.S., 1987. Population balance modeling of the dissolution of polydisperse solids: Rate limiting regimes. AIChE J. 33, 54–63.
LeBlanc, S.E., Fogler, H.S., 1989. Dissolution of powdered minerals: The effect of polydispersity. AIChE J. 35, 865–868.
Levenspiel, O., Wiley, J., Hepburn, K., Levenspiel, O., 1999. Chemical Reaction Engineering - third edition, 3th edition.
Levins, D.M., Glastonbury, J.R., 1972. Application of Kolmogorofff's theory to particle-liquid mass transfer in agitated vessels. Chem. Eng. Sci. 27, 537–543.
Luo, H., Svendsen, H.F., 1996. Theoretical Model for Drop and Bubble Breakup in Turbulent Dispersions. AIChE J. 42, 1225–1233.
Marchisio, D.L., Fox, R.O., 2013. Computational Models for Polydisperse Particulate and Multiphase Systems, Cambridge University Press. New York.
Marchisio, D.L., Vigil, R.D., Fox, R.O., 2003. Quadrature method of moments for aggregation-breakage processes. J. Colloid Interface Sci. 258, 322–334.
Marquardt, D.W., 1963. An Algorithm for Least-Squares Estimation of Nonlinear Parameters. J. Soc. Ind. Appl. Math. 11,431–441.
Newman, J.S., 1991. Electrochemical systems. Prentice Hall, New Jersey.

Noyes, A.A., Whitney, W.R., 1897. The rate of solution of solid substances in their own solutions. J. Am. Chem. Soc. 19, 930–934.

Paul, E.L., Atiemo-Obeng, V.A., Kresta, S.M., 2004. Handbook of industrial mixing : science and practice, 1st ed. Wiley-Interscience, New Jersey.

Peng, S.J., Williams, R.A., 1994. Direct Measurement of Floc Breakage in Flowing Suspensions. J. Colloid Interface Sci. 166, 321–332.

Randolph, A.D., Larson, M.A., 1988. Theory of particulate processes : analysis and techniques of continuous crystallization. Academic Press.

Tinoco, I., Sauer, K., Wang, J.C., 1995. Physical chemistry : principles and applications in biological sciences. Prentice Hall, New Jersey.

Vanni, M., 2000. Approximate Population Balance Equations for Aggregation-Breakage Processes. J. Colloid Interface Sci. 221, 143–160.

Zaccone, A., Gäbler, A., Maaß, S., Marchisio, D., Kraume, M., 2007. Drop breakage in liquid–liquid stirred dispersions: Modelling of single drop breakage. Chem. Eng. Sci. 62, 6297–6307.

Zhao, W., Buffo, A., Alopaeus, V., Han, B., Louhi-Kultanen, M., 2017. Application of the compartmental model to the gas-liquid precipitation of CO 2 -Ca(OH) 2 aqueous system in a stirred tank. AIChE J. 63, 378–386.

Zhao, W., Han, B., Jakobsson, K., Louhi-Kultanen, M., Alopaeus, V., 2016. Mathematical model of precipitation of magnesium carbonate with carbon dioxide from the magnesium hydroxide slurry. Comput. Chem. Eng. 87, 180–189.